Molecules and Cells

Intramolecular Disulfide Bonds for Biogenesis of CALHM1 Ion Channel Are Dispensable for Voltage-Dependent Activation

Jae Won Kwon[1,2,4], Young Keul Jeon[1,2,4], Jinsung Kim[1,2], Sang Jeong Kim[1,2], and Sung Joon Kim[1,2,3,*]

[1]Department of Physiology, Seoul National University College of Medicine, Seoul 03080, Korea, [2]Department of Biomedical Sciences, Seoul National University College of Medicine, Seoul 03080, Korea, [3]Ischemic/Hypoxic Disease Institute, Seoul National University College of Medicine, Seoul 03080, Korea, [4]These authors contributed equally to this work.
*Correspondence: physiolksj@gmail.com
https://doi.org/10.14348/molcells.2021.0131
www.molcells.org

Calcium homeostasis modulator 1 (CALHM1) is a membrane protein with four transmembrane helices that form an octameric ion channel with voltage-dependent activation. There are four conserved cysteine (Cys) residues in the extracellular domain that form two intramolecular disulfide bonds. We investigated the roles of C42-C127 and C44-C161 in human CALHM1 channel biogenesis and the ionic current (I_{CALHM1}). Replacing Cys with Ser or Ala abolished the membrane trafficking as well as I_{CALHM1}. Immunoblotting analysis revealed dithiothreitol-sensitive multimeric CALHM1, which was markedly reduced in C44S and C161S, but preserved in C42S and C127S. The mixed expression of C42S and wild-type did not show a dominant-negative effect. While the heteromeric assembly of CALHM1 and CALHM3 formed active ion channels, the co-expression of C42S and CALHM3 did not produce functional channels. Despite the critical structural role of the extracellular cysteine residues, a treatment with the membrane-impermeable reducing agent tris(2-carboxyethyl) phosphine (TCEP, 2 mM) did not affect I_{CALHM1} for up to 30 min. Interestingly, incubation with TCEP (2 mM) for 2-6 h reduced both I_{CALHM1} and the surface expression of CALHM1 in a time-dependent manner. We propose that the intramolecular disulfide bonds are essential for folding, oligomerization, trafficking and maintenance of CALHM1 in the plasma membrane, but dispensable for the voltage-dependent activation once expressed on the plasma membrane.

Keywords: CALHM1, disulfide bond, membrane trafficking, oligomerization, reducing agent

INTRODUCTION

Calcium homeostasis modulator 1 (CALHM1) is a newly identified voltage-gated nonselective ion channel, and its functional expression has been reported in cerebral cortical neuronal cells and taste bud cells (Dreses-Werringloer et al., 2008; Taruno et al., 2013). In cerebral neurons, CALHM1 is reportedly involved in the action potential frequency-dependent regulation of excitability (Vingtdeux et al., 2016). In type II taste bud cells, CALHM1 interacts with CALHM3 as a pore-forming subunit, and the CALHM1/3 hetero-multimeric channel functions as an endogenous ATP-release channel signaling to the purinoceptors in the sensory nerve ending (Kashio et al., 2019; Ma et al., 2018).

In whole-cell patch clamp studies, CALHM1-expressing cells showed slowly activating outward currents under strong depolarized conditions, and the voltage-dependence was shifted to the left by lowering the extracellular Ca^{2+} concen-

Received 20 May, 2021; revised 19 August, 2021; accepted 6 September, 2021; published online 29 October, 2021

eISSN: 0219-1032

tration ($[Ca^{2+}]_e$) (Ma et al., 2012). We have recently reported that both voltage dependence and activation speed were markedly potentiated by raising the temperature to physiological ranges (Jeon et al., 2021). Also, CALHM1 current activation shows tendency of sensitization by repetitive stimuli as like the voltage-dependent activation of Anoctamin 6/TMEM16F (Roh et al., 2021).

All six paralogues of the CALHM family proteins have four transmembrane domains with both N-and C-termini located on the cytoplasmic side. Recent cryo-EM studies have revealed octameric (CALHM1) and undecameric (CALHM2 and 4) assemblies with wide pore diameters consistent with the unselective permeability to various ion sizes, including ATP^{4-} (Choi et al., 2019; Drozdzyk et al., 2020; Foskett, 2020; Syrjanen et al., 2020). There are four strictly conserved cysteine residues in the extracellular domains of human CALHM1, CALHM2, and CALHM3 (Figs. 1A and 1B). Based on the cryo-EM study, the conserved C42, C44, C127, and C161 residues in CALHM1 are linked by disulfide bonds (C42-C127 and C44-C161) (Demura et al., 2020; Ren et al., 2020) (Figs. 1C-1E). The supplementary data from a study of *Caenorhabditis elegans* calhm1 suggested a critical role for the disulfide bonds in membrane expression (Yang et al., 2020). However, their role in mammalian CALHM1 has not yet been confirmed. Furthermore, the putative sensitivity of CALHM1 in reducing the environment through the state of disulfide bonds has not yet been investigated.

The roles of intramolecular (between protein domains) and intermolecular (units of multimeric assemblage) disulfide bonds vary depending on the biogenesis, trafficking, and gating mechanisms (see Discussion section). Therefore, it is critical to elucidate the structural and functional roles of disulfide bonds in newly identified ion channels such as CALHM1. In the present study, we investigated the role of two disulfide bridges in the extracellular domains of human CALHM1 overexpressed in CHO cells. All four Cys mutants completely lost their channel activity and membrane expression. Although the disulfide bond breakage using the reducing agents dithiothreitol (DTT) and tris(2-carboxyethyl) phosphine (TCEP) did not acutely change the channel activity, sustained treatment with TCEP (≥2 h) significantly reduced I_{CALHM1} and membrane expression. These results indicate that two disulfide bonds between conserved extracellular cysteine residues are essential for the proper folding for oligomerization and trafficking but are dispensable for the electrophysiological function of CALHM1 once it is localized to the plasma membrane.

MATERIALS AND METHODS

Cell culture preparation

Chinese hamster ovary (CHO) and human embryonic kidney cell line (HEK293) cells were purchased from ATCC (USA) and incubated in Dulbecco's modified Eagle's medium (DMEM; Gibco, USA) supplemented with 10% fetal bovine serum (FBS; Gibco) and 1% penicillin-streptomycin (Gibco). The cells were incubated at 37°C and 5% CO_2. The cells were sub-cultured by centrifuging at 160 × *g* for 2 min and then trypsinized. CHO cells at less than 30 passages were used for subsequent experiments because of the very low expression of endogenous ion channels (Gamper et al., 2005).

Molecular cloning and heterologous expression of CALHM1

To insert the coding sequence (CDS), the cDNA of human CALHM1 and pEGFP-N1 vector (Takara Bio, USA) were truncated with the restriction enzymes *Eco*RI and *Bam*HI. Truncated inserts were ligated, and the sequence of the CALHM1-EGFP vector was confirmed. All point mutations in CALHM1 were generated and PCR-amplified using the QuikChange II site-directed mutagenesis kit (Agilent Technologies, USA), and the sequences of eight mutants were confirmed by DNA sequencing. All constructs were transfected into CHO cells using the TurboFect transfection reagent (Thermo Fisher Scientific, USA) according to the manufacturer's protocol. The day before transfection, 3×10^4 cells were seeded on a 12-well culture dish. The following day, 300 ng of the CALHM1-EGFP vector was transfected into the cells in each well. Downstream experiments were conducted 18-40 h after transfection. For co-immunoprecipitation, the FLAG (DYKDDDDK) tag and stop codon were inserted between the CALHM1 and EGFP using Gibson assembly method (Gibson et al., 2009). HEK293 cells (3×10^5 cells) were seeded on 6-well dishes and co-transfected CALHM1-FLAG with WT CALHM1-EGFP or C42S CALHM1-EGFP (total amount of cDNA was 1 μg) using the Lipofectamine 3000 (Thermo Fisher Scientific) according to the manufacturer's protocol.

Electrophysiology

The transfected CHO cells were transferred to a bath mounted on the stage of an inverted microscope (*Ti;* Nikon, Japan). Borosilicated glass pipettes were connected to the CV 203BU head stage of a patch-clamp amplifier (Axopatch 200B; Axon Instruments, USA). The current was recorded at 10 kHz and low-pass Bessel-filtered at 5 kHz. pCLAMP software version 10.6.2, and Digidata-1440A (Axon Instruments) were used to acquire data and apply command pulses. Data were processed using Clampfit version 11.2 (Axon Instruments). The temperature of the bath and cells was controlled using an in-line solution heating system (Warner Instruments, USA), which was placed in front of the bath. The temperature was monitored using a thermistor in the bath near the cells (<300 μm) and recorded using a digitizer. Pipettes with a free-tip resistance of 2.0-2.8 MΩ were used for whole-cell patch clamp. Series resistance was estimated by dividing the time constants of the capacitive current with the membrane capacitance, which was kept below 10 Ω in the whole-cell configuration. Because the electrical capacitance of the cell reflects the surface area of the plasma membrane, the current density of I_{CALHM1} was defined as the amplitude of the time-dependent outward current component divided by the cell capacitance ($pA \cdot pF^{-1}$). The bath was continuously perfused at a constant flow rate ($5\ ml \cdot min^{-1}$) with Normal Tyrode's bath solution (NT) comprised of (in mM) 140 NaCl, 5.4 KCl, 2 $CaCl_2$, 1 $MgCl_2$, 10 glucose, 20 mannitol, and 10 HEPES [4-(2-hydroxyethyl)-1-piperazine ethanesulfonic acid], pH 7.4 (titrated with NaOH) for whole-cell patch clamp experiments. The Ca^{2+} concentration of NT was modified based on the experimental conditions (0 and 2 mM). The pipette solution

used for whole-cell patch clamp contained (in mM) 140 CsCl, 0.5 $MgCl_2$, 10 EGTA [ethylene glycol-bis(β-aminoethyl ether)-*N,N,N',N'*-tetra acetic acid], and 10 HEPES, pH 7.2 (titrated with CsOH). A salt-agar bridge with 3 M KCl was used to compensate for the junction potential change following treatment with reducing agents (Berman and Awayda, 2013). The reagents used in this study were purchased from Sigma-Aldrich (USA).

Confocal microscopy imaging

CALHM1-overexpressed cells were imaged on an 18 mm coverslip with an A1 confocal microscope (Nikon) one day after transfection. Cell-attached coverslips were fixed with 4% paraformaldehyde and washed three times with ice-cold phosphate-buffered saline (PBS). The membranes and nucleus of cells were stained in the dark using 5 μg/ml wheat germ agglutinin (WGA) and 1 μg/ml 4′,6-diamidino-2-phenylindole (DAPI), respectively. Images were scanned with a 100× immersion objective lens at 512 × 512 pixels using a digital zoom. All confocal images were processed and transferred using NIS software (Nikon) and ImageJ software (NIH, USA).

Immunoblotting and surface biotinylation

Proteins were extracted from overexpressed CHO cells using lysis buffer containing 0.5 M EDTA, 25 mM Tris-HCl, 150 mM NaCl, and 1% Triton X-100 with a phosphatase and protease inhibitor cocktail (Roche, Germany), pH 7.4. After scraping the cells and treating them with the lysis buffer, the lysates were homogenized 10 times with a sterile 26-gauge needle. The protein was quantified using the Bradford assay (Bio-Rad, USA). After incubation at 95°C with an appropriate concentration of DTT (indicated in the results), lysates were fractionated using SDS-PAGE on 3%-8% gradient gels (Thermo Fisher Scientific) and transferred onto a PVDF membrane in 25 mM Tris, 192 mM glycine, and 20% methanol. Membranes were blocked with 5% skim milk containing 1% TBS and Tween-20 (TBS-T) for 4 h at room temperature, with gentle rocking. Membranes were then incubated overnight at 4°C with anti-GFP (Invitrogen, USA) and anti-GAPDH (USA) primary antibodies, and this was followed by incubation with secondary antibodies after washing three times with TBS-T. Blots were developed using ECL Plus western blotting detection reagents (Merck, Germany) for western blot analysis.

To detect CALHM1 in the surface membrane fraction, CHO cells were washed with ice-cold PBS and incubated in 0.5 mg/well Sulfo-NHS-SS-Biotin (Thermo Fisher Scientific) for 1 h at 4°C. Unreacted biotin was quenched using 50 mM Tris (pH 7.4) and washed with ice-cold PBS. Biotinylated proteins were then extracted as described above. Avidin slurry (100 μl; Thermo Fisher Scientific) was added to 500 μl of cell lysate (500 μg of biotinylated protein) in spin columns and incubated, with rotation, for 1 h at room temperature. After washing the beads three times with TBS-T, proteins were eluted with elution buffer (62.5 mM Tris, 1% SDS, 10% glycerol, and 50 mM DTT). The eluted proteins were fractionated using SDS-PAGE on 4%-12% gradient gels and immunoblotted as described above.

Co-immunoprecipitation

To explore the biochemical interaction of WT CALHM1 and C42S CALHM1, after co-transfection for 24 h, cells were washed with ice-cold PBS and harvested in lysis buffer (120 mM NaCl, 50 mM HEPES, 2 mM EDTA, 2 mM $MgCl_2$, and 0.5% Triton X-100 with a phosphatase and protease inhibitor cocktail, pH 7.4). The lysates were passed 17 times through a sterile 26-gauge needle and incubated on a rotator for 30 min at 4°C. After centrifugation, the protein concentration in the supernatants were measured and 200 μg of lysates (500 μl) were incubated with 30 μl of Protein G-agarose beads (Thermo Fisher Scientific) coupled to 1 μg of anti-FLAG M2 antibody (Sigma-Aldrich) or anti-GFP antibody (Thermo Fisher Scientific) on a rotator at 4°C overnight. After beads were washed twice with wash buffer and once with ice-cold PBS, the precipitates were eluted with 25 μl of 2× sample buffer (120 mM Tris-Cl, 4% SDS, 0.02% bromophenol blue, 20% glycerol, 10 mM DTT) at 60°C for 5 min. The lysates for input (10 μg) were incubated in sample buffer at 95°C for 5 min. All samples were fractionated using SDS-PAGE on 4%-12% gradient gels and immunoblotted as described above.

Statistical analysis and data presentation

Statistical analysis was performed using Origin Pro 2021 (OriginLab Corporation, USA) and Prism 9.2.0 (GraphPad Software, USA). Data are presented as the mean ± SD. Student's unpaired *t*-test and one-way ANOVA were used where appropriate, and differences were considered significant at $P < 0.05$. Multiple protein sequence alignments were performed using the modified ClustalW algorithm (Thompson et al., 1994). Homology modeling was performed using the SWISS-MODEL workspace, based on the cryo-EM structure of CALHM2 (Choi et al., 2019; Waterhouse et al., 2018). Structural analysis was performed based on the published cryo-EM structure of killifish calhm1 (Demura et al., 2020). The killifish calhm1 structure was visualized using PyMOL (Schrödinger, USA).

RESULTS

The schematic figure of barrels and connecting lines demonstrates the topology and domains of CALHM1 (Fig. 1A). Amino acid sequences of the three human CALHM paralogues (CALHM1-3) and the calhm1 sequences of mice and killifish were compared (Fig. 1B). Four cysteine residues (C42, C44, C127, and C161 in human CALHM1) were conserved across all five proteins. The densities of the two disulfide bonds between the conserved cysteines (C42-C127 and C44-C161) in the killifish calhm1 cryo-EM structure were determined (Figs. 1C-1E). All these residues were located in the extracellular space, and the two disulfide bonds were located relatively close to each other (Figs. 1C and 1D, red color). Since the cryo-EM structure of human CALHM1 has not been reported before, we used the homologous model to confirm whether the less-conserved cysteine molecules also formed disulfide bonds. There were eight additional cysteine residues in cryo-EM structure, but they were too far from each other to form disulfide bonds (Fig. 1D, orange color). Taken together, we confirmed that only the four conserved cysteine residues

formed the two disulfide bonds identified (Fig. 1E).

We compared the electrophysiological properties of cysteine mutants and wild-type (WT) CALHM1 in CHO cells. In the whole-cell patch clamp configuration, step-like depolarization was applied from –40 mV of holding voltage to 80 mV (5 s) with various levels, followed by repolarization to –40 mV. At room temperature, slowly activating outward currents (I_{CALHM1}) were observed only at strong depolarizations above 40 mV (Fig. 2A, left panel) but not in the empty CHO cells (data not shown). Consistent with the known CALHM1 property (Ma et al., 2012; Tanis et al., 2017), removal of extracellular Ca^{2+} ($[Ca^{2+}]_e$) facilitated voltage-dependent activation of CALHM1 current (Fig. 2A, middle panel). We recently reported on the thermosensitivity of CALHM1 (Jeon et al., 2021) and confirmed the significant facilitation of CALHM1 activation at physiological temperature (37°C, Fig. 2A, right panel). The summarized results are presented as current-to-voltage relations (I-V curves, Fig. 2B). The voltage dependence of CALHM1 current was investigated with conductance-to-voltage relations (G-V curves, Fig. 2C) under three conditions as described above. The voltage was stepped from –40 mV to 120 mV (2 s) with 10 mV increments, followed by repolarization to –80 mV (1 s) and then back to –40 mV of holding potential. By removing the $[Ca^{2+}]_e$ or increasing the temperature to 37°C, the half-maximal activation voltage ($V_{1/2}$) was shifted to the left (42.90 ± 2.515 mV, 58.25 ± 0.725 mV, re-

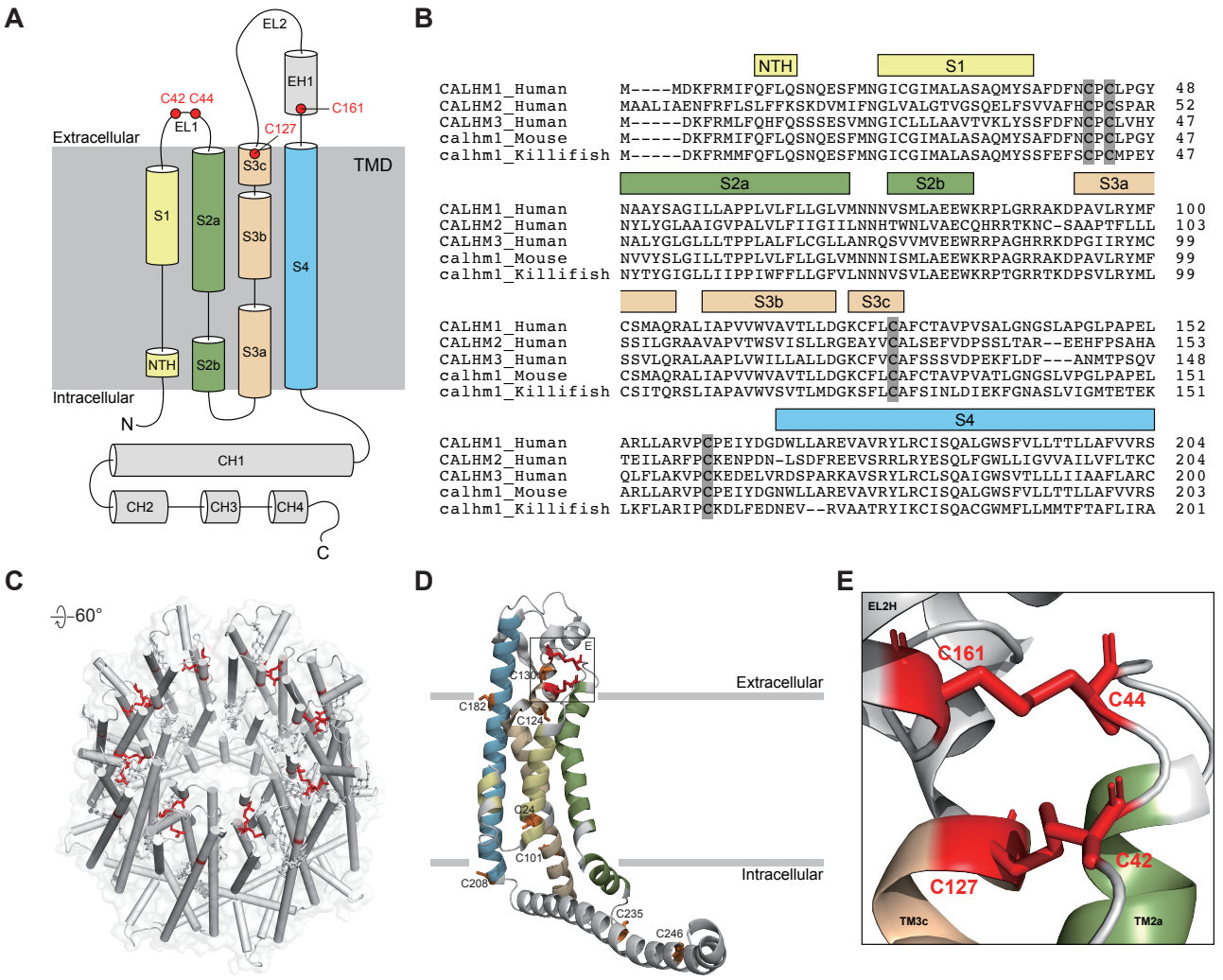

Fig. 1. CALHM1 protein sequence and structure. (A) Schematic topology of CALHM1 showing four transmembrane domains (TMD), two extracellular loops (EL), short N-terminal helix (NTH), and four C-terminal helices (CH1-4). The four conserved cysteine residues are presented as red dots; C42 and C44 in EL1, C127, and C161 in EL2. (B) Amino acid sequences of human CALHM1-3, mouse calhm1, and killifish calhm1 were aligned using the Clustal Omega algorithm. The four cysteine residues are highlighted within grey boxes. (C) The octameric structure of killifish calhm1 is depicted, and the locations of conserved cysteine residues are highlighted in red color (PDB accession code: 6LMT). (D) A three-dimensional drawing of CALHM1 monomer; colored ribbon-type representation of domains is similar to that in (A). The locations of eight non-conserved cysteine residues are highlighted in orange color. (E) Magnified view of the two disulfide bonds: C42-C127 and C44-C161 (red color).

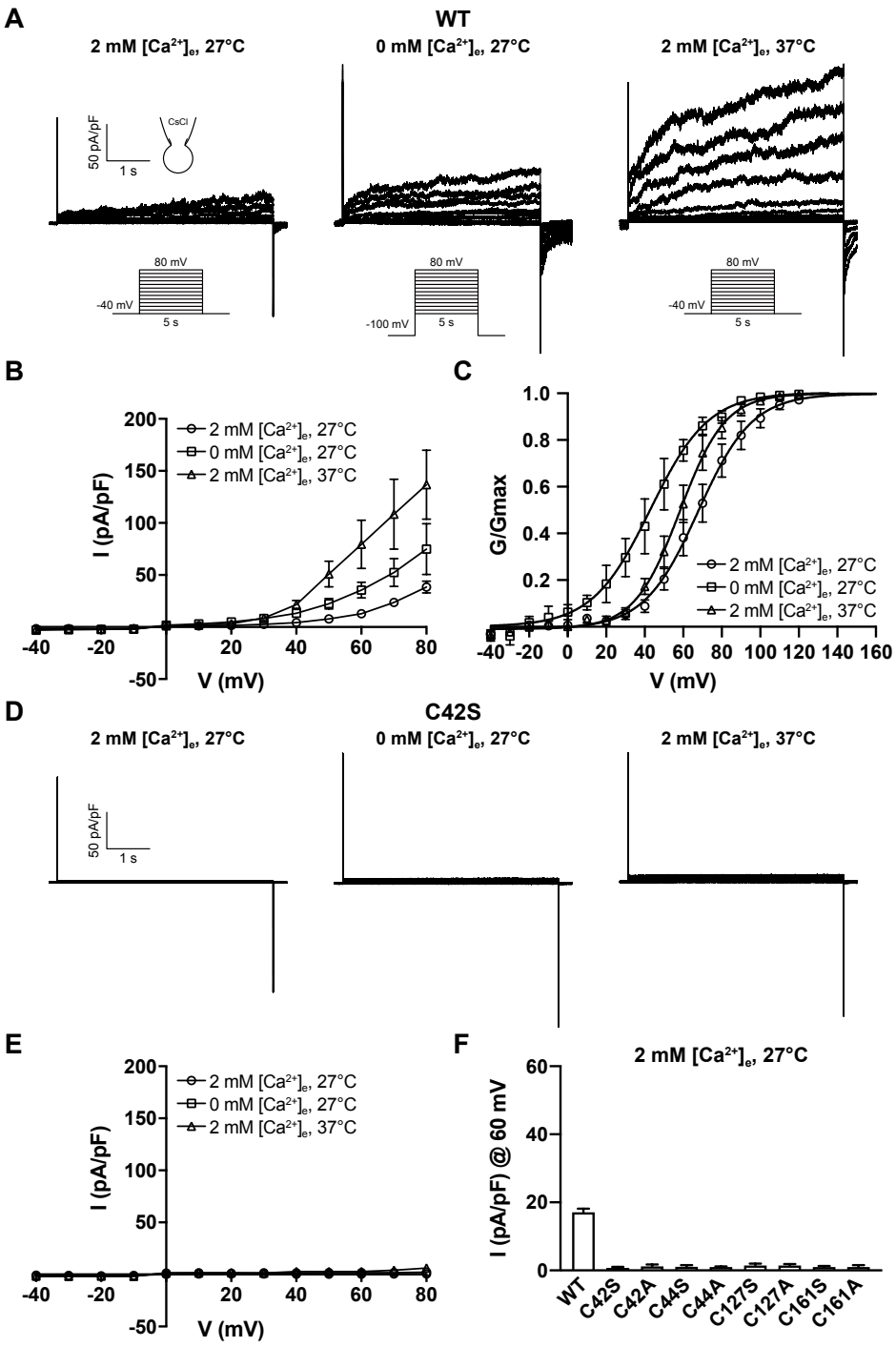

Fig. 2. Electrical activity of CALHM1 and loss of function in Cys mutants. (A) Representative traces of WT CALHM1 current activated by step-like depolarizations ranging from -40 to 80 mV (5 s) every 20 s under standard condition (2 mM $[Ca^{2+}]_e$ and 27°C), nominal Ca^{2+}-free, and at 37°C. (B and C) I-V curves and G-V curves of WT obtained under the three conditions (n = 12 and 10-12 for I-V curves and G-V curves, respectively). (D) No current was observed in cells expressing C42S. (E) I-V curves of C42S obtained under the three conditions (n = 6-8). (F) Summary of current densities of wild-type CALHM1 (n = 64) and all the cysteine mutants under standard condition (n = 4-6).

spectively) compared with condition of 2 mM $[Ca^{2+}]_e$ at room temperature (67.76 ± 0.965 mV).

Replacement of any of the four cysteines residues with serine or alanine residues by site-directed mutagenesis completely abolished I_{CALHM1}. Representative patch clamp recordings of CHO cells transfected with C42S at room temperature, free calcium (0 mM $[Ca^{2+}]_e$), and at 37°C are shown in Figs. 2D and 2E. In addition, the summary of outward current densities at 60 mV in CHO cells expressing the tested mutants is shown as bar graphs (Fig. 2F), clearly indicating the loss of channel function across all the mutations.

To investigate CALHM1 trafficking to the plasma membrane, we conducted confocal microscopic analysis of CHO cells expressing CALHM1 with an EGFP tag (Figs. 3A and 3B). The cells were co-stained with WGA, which binds to the glycoproteins in the cell membrane (Fig. 3A, red color). Wild-type CALHM1 was localized to the plasma membrane, along with the puncta form of intracellular expression (Fig.

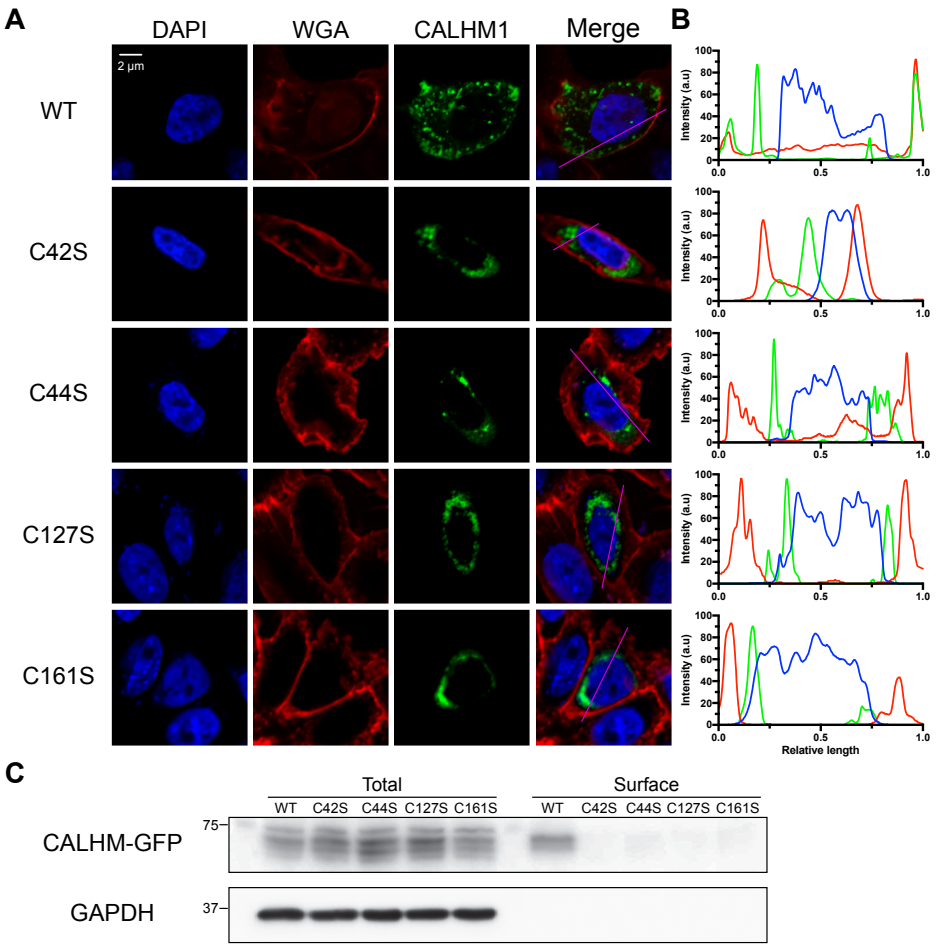

Fig. 3. Surface expression of CALHM1 and cysteine mutants. (A) Representative confocal images of CHO cells expressing the wild-type CALHM1 (uppermost row) and four cysteine-to-serine mutants are shown. Four images are shown per row for each cell, with the blue DAPI fluorescent signal shown in the first column, the red WGA signal of plasma membrane in the second column, the green CALHM1-associated signal in the third column, and the merged signal shown in the fourth column. Despite the considerable portion of wild-type CALHM1 proteins expressed in the cytosolic space, distinct membrane expression of CALHM1 was confirmed in yellow-colored regions. (B) Line scanning of fluorescent images was processed using ImageJ software. (C) Surface expression was confirmed using surface biotinylation followed by immunoblotting. The total and surface represented whole cell lysate and surface fraction, respectively.

3A, uppermost panel). Notably, a considerable amount of the CALHM1 protein was located in the perinuclear region. A pattern of relatively larger cytosolic expression of WT CALHM1 has also been reported (Dreses-Werringloer et al., 2008). In contrast to WT, none of the Cys mutants showed plasma membrane localization, while the perinuclear expression pattern was evident (Figs. 3A and 3B). We also compared the plasma membrane expressions of WT with the expression of cysteine mutants using a surface biotinylation technique. While WT CALHM1 was found in the plasma membrane fraction, none of the four cysteine mutants were detected (Fig. 3C). The multi-bands of WT and Cys mutants in the whole-cell lysates indicate variations of *N*-glycochains on CALHM1, as reported by Okui et al. (2021).

We then evaluated whether intramolecular disulfide bonds are necessary for multimerization in the biogenesis of the CALHM1 channel. Immunoblotting using 3%-8% polyacrylamide gels was performed with or without a reducing agent (DTT, 0, 0.1, 1, and 10 mM). In the control condition, CALHM1 proteins of various sizes were detected, pointing to the presence of monomers, dimers, and tetramers (Fig. 4A). The calculated molecular weight of CALHM1-GFP is ~65.9 kDa, and the predicted molecular masses for dimeric and tetrameric forms are ~131.8 kDa and ~263.6 kDa, respectively. The multimeric forms of CALHM1 decreased with increasing concentrations of DTT, while the monomeric form increased. When either C42 or C127 was replaced with serine, multimeric bands were detected in the non-reducing condition (0 mM DTT), similar to WT (Fig. 4B). In contrast, the multimeric sizes of C44S and C161S decreased significantly, even under non-reducing conditions. We compared the intensity of monomer and tetramer bands in four immunoblots with increasing concentrations of DTT. Whereas the relative expression ratios of monomer gradually increased to 3.24 at 10 mM DTT in WT, those of tetramer decreased to 0.22, when normalized to signal intensity of 0 mM DTT (Fig. 4C). The ratios of monomer and tetramer bands in C42S and C127S were similar to WT (monomers, 3.12 and 2.97; tetramers, 0.28 and 0.14, respectively, Fig. 4D), while not significantly altered in C44S and C161S (monomers, 1.53 and 1.44; tetramers, 0.55 and 0.67, respectively).

Co-expression of WT with mutated channel units often showed dominant-negative effects, and hetero-multimerized channels showed impaired electrophysiological function (Bannister et al., 1999; Cho et al., 2000). Since the functional CALHM1 channel has an octameric structure, a putative hetero-multimeric assembly might disrupt the function of the channel. When WT and C42S cDNAs were co-transfected using constant quantities of WT and increasing quantities of C42S (10:1, 10:2, 10:5, and 10:10), the I_{CALHM1} amplitude did

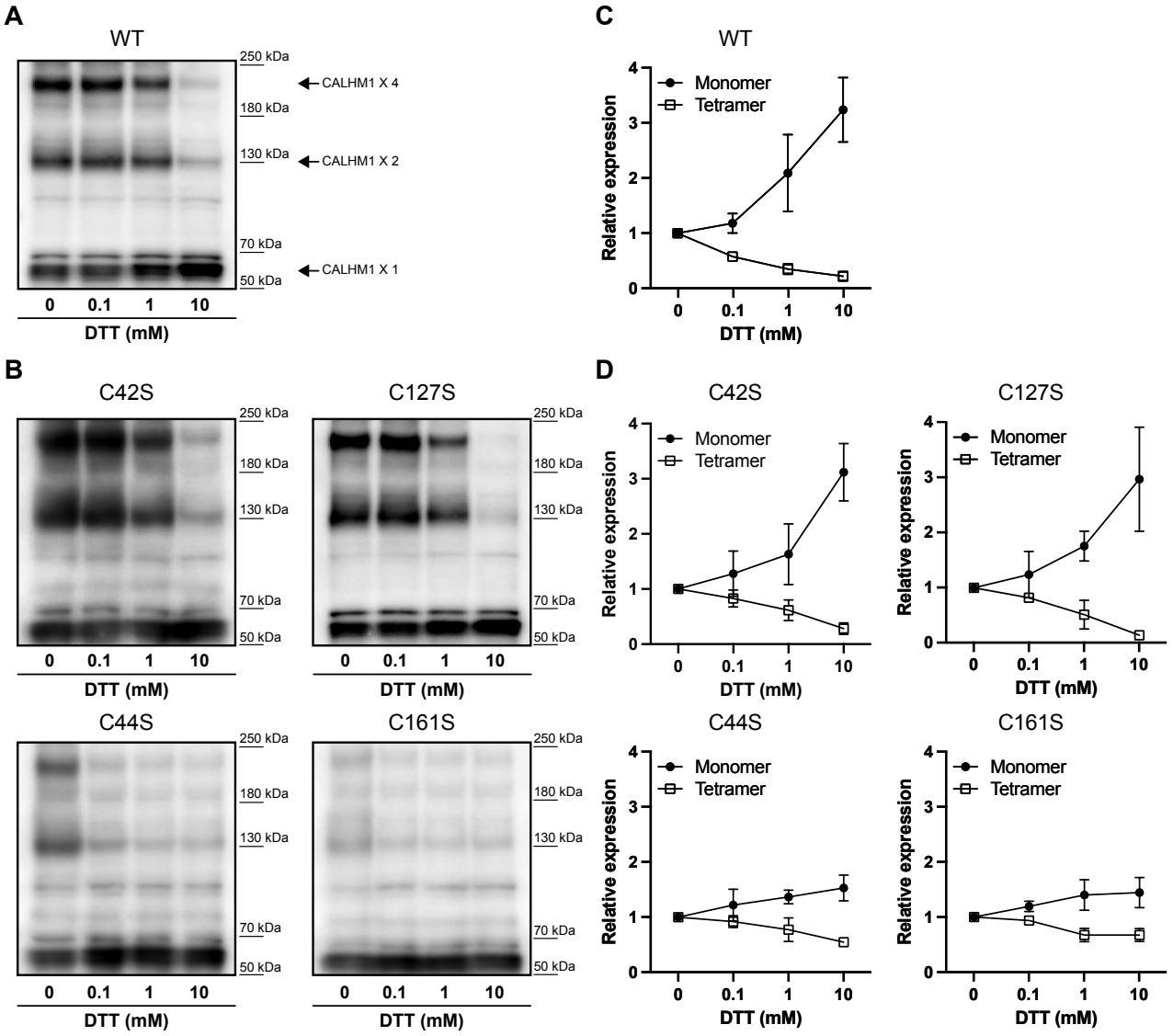

Fig. 4. Multimeric formation of wild-type CALHM1 and cysteine mutants. (A) 10 μg of freshly prepared cell lysate from wild-type CALHM1-transfected CHO cells was solubilized in SDS sample buffer without (lane 1) or with DTT (0.1, 1, and 10 mM, lanes 2-4), followed by separation on SDS-PAGE and immunoblotting using GFP-antibodies. The predicted molecular weight for monomeric, dimeric, and tetrameric forms of CALHM1 are marked with arrows on the right side. (B) Immunoblotting of four cysteine-to-serine mutants was performed. The oligomerization of the ion channel was reduced in two cysteine mutants (C44S and C161S) but not in the other two mutants (C42S and C127S). (C) Relative immunoreactive band intensities of monomer and tetramer in WT without or with DTT. (D) The expressions pattern of monometric- or tetrametric form were altered in C42S and C127S comparing with WT, while not in C44S and C161S according to the concentrations of DTT.

not change significantly (Fig. 5A). Furthermore, when the total amount of transfected cDNA was kept constant, the increased ratio of C42S (9:1, 1:1, and 1:9) induced only a gradual decrease in I_{CALHM1}. Notably, the current density was still significant even when the ratio of WT and C42S cDNA was 1:9 (30 ng:270 ng).

To determine whether WT and C42S CALHM1 form hetero-multimerized channels, we performed co-expression and immunoprecipitation of FLAG tagged WT CALHM1 and GFP tagged C42S CALHM1 cDNAs with a positive control expressed with different (FLAG or GFP) tagged WT CALHM1 cDNAs. While CALHM1 co-immunoprecipitates with itself as a homo-multimer, GFP tagged C42S CALHM1 was not pulled down with FLAG tagged WT CALHM1, indicating C42S CALHM1 could not interact with WT CALHM1 (Fig. 5B).

The intrinsically expressed ATP-releasing channel in taste buds is composed of CALHM1 and CALHM3 (Kashio et al., 2019; Ma et al., 2018). When expressed with CALHM3 alone, CHO cells showed negligible voltage-dependent currents (Fig. 5C). However, when co-expressed with CALHM1,

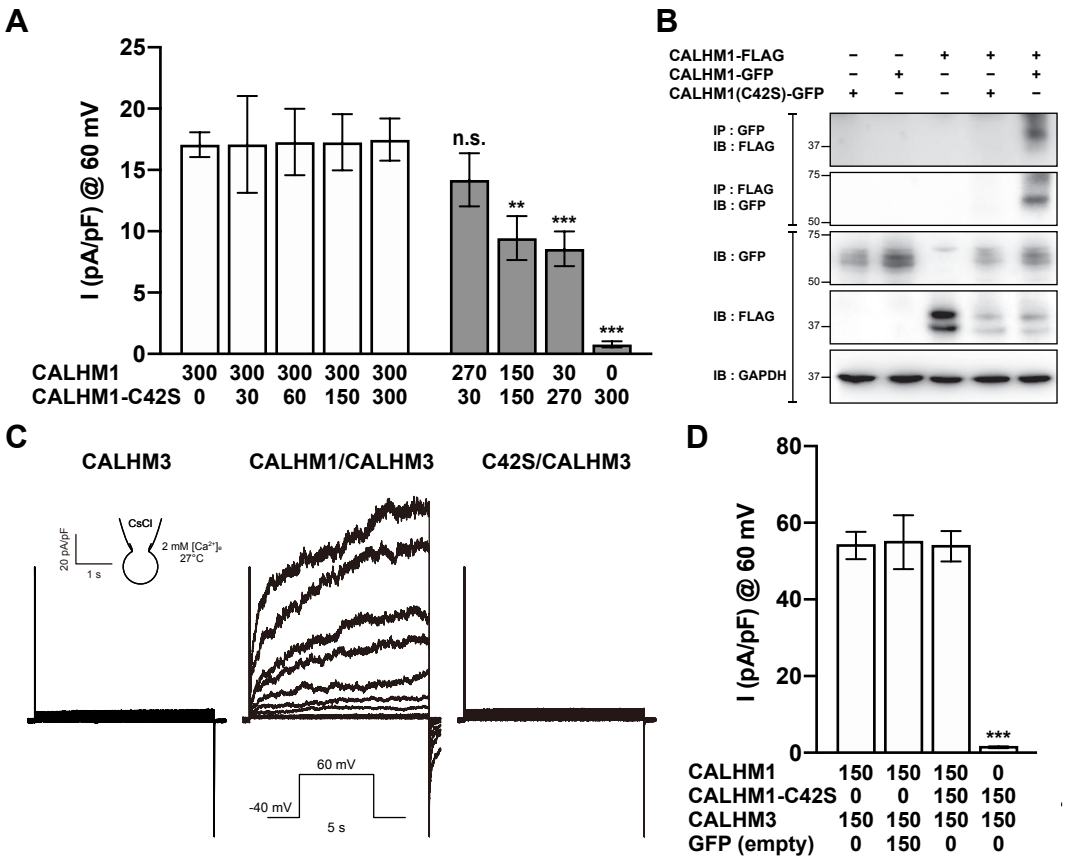

Fig. 5. No interaction of cysteine mutants and WT CALHM1. (A) Wild-type CALHM1 cDNA was injected alone or with C42S mutant cDNA. The ratios of WT CALHM1 and C42S cDNA were 10:0, 10:1, 10:2, 10:5, and 10:10 (n = 5-9). The current densities did not differ between the groups (open bars). In addition, a combination of WT CALHM1 and C42S cDNA was transfected into CHO cells with varying amounts (9:1, 1:1, 1:9), which of the total amount was 300 ng (n = 11-15). I_{CALHM1} decreased based on the amount of wild-type vector (**$P < 0.01$, ***$P < 0.001$, grey bars). n.s., not significant. (B) Co-immunoprecipitation blot represents that C42S CALHM1 do not interacts with WT CALHM1. CALHM1 interacts with itself, but could not assemble with C42S CALHM1 through hetero-multimerization. (C) Representative traces of the currents recorded in CHO cells expressing CALHM3 alone and co-expression of CALHM1/CALHM3 or C42S/CALHM3 under standard condition (2 mM $[Ca^{2+}]_e$ and 27°C). (D) Summary of the membrane current densities in CHO cells co-expressing CALHM3, WT CALHM1 and C42S cDNA. The current densities of triple co-expression of CALHM1, C42S, and CALHM3 did not differ from that of CALHM1, CALHM3, and GFP (n = 5). In contrast, the co-expression of C42S with CALHM3 did not show significant current (n = 7). ***$P < 0.001$.

the voltage-dependent outward $I_{CALHM1/3}$ showed a larger amplitude (54.5 ± 3.57 pA/pF), with faster kinetics of activation compared with I_{CALHM1} (Figs. 5C and 5D). These results are consistent with previous reports (Ma et al., 2018). The co-expression of CALHM3 with C42S CALHM1 could not rescue the electrophysiological activity; no outward voltage-dependent current was observed (Figs. 5C and 5D). Although the data obtained from the co-expression of WT CALHM1 and C42S excluded any interaction between the two, the significant $I_{CALHM1/3}$ compared with I_{CALHM1} might suggest a rescue effect from WT to C42S through hetero-multimerization. To test this hypothesis, the current density of triple co-expression of WT, C42S CALHM1, and CALHM3 was compared with that of WT CALHM1 and CALHM3 and with GFP, replacing the C42S cDNA. Including C42S did not affect $I_{CALHM1/3}$ amplitude, similar to GFP (empty vector), suggesting that the CALHM1 cysteine mutant did not assemble into the CALHM1/3 hetero-multimeric channel (Fig. 5D).

Finally, we investigated whether reducing agents used to break the cysteine bridges could affect CALHM1 activity. Step depolarization from −40 to 60 mV (5 s) was repetitively applied to activate CHO cells expressing WT CALHM1 every 30 s. After confirming the constant amplitudes of I_{CALHM1}, 2 mM DTT or TCEP was added to the bath perfusing solution, and this did not significantly change I_{CALHM1} amplitude for up to 30 min (Figs. 6A and 6B). Treatment with 10 μM ruthenium red or 10 μM Gd^{3+}, known blockers of CALHM1, almost completely suppressed I_{CALHM1} (data not shown). In contrast to the acute effect of the reducing agents, prolonged pretreatment (2-6 h) of the transfected cells with 2 mM TCEP significantly reduced I_{CALHM1} amplitude compared with time-matched control cells (Fig. 6C). I_{CALHM1} suppression by TCEP pretreatment suggests reduced membrane expression (internalization) or degradation of the CALHM1 protein. In fact, based on

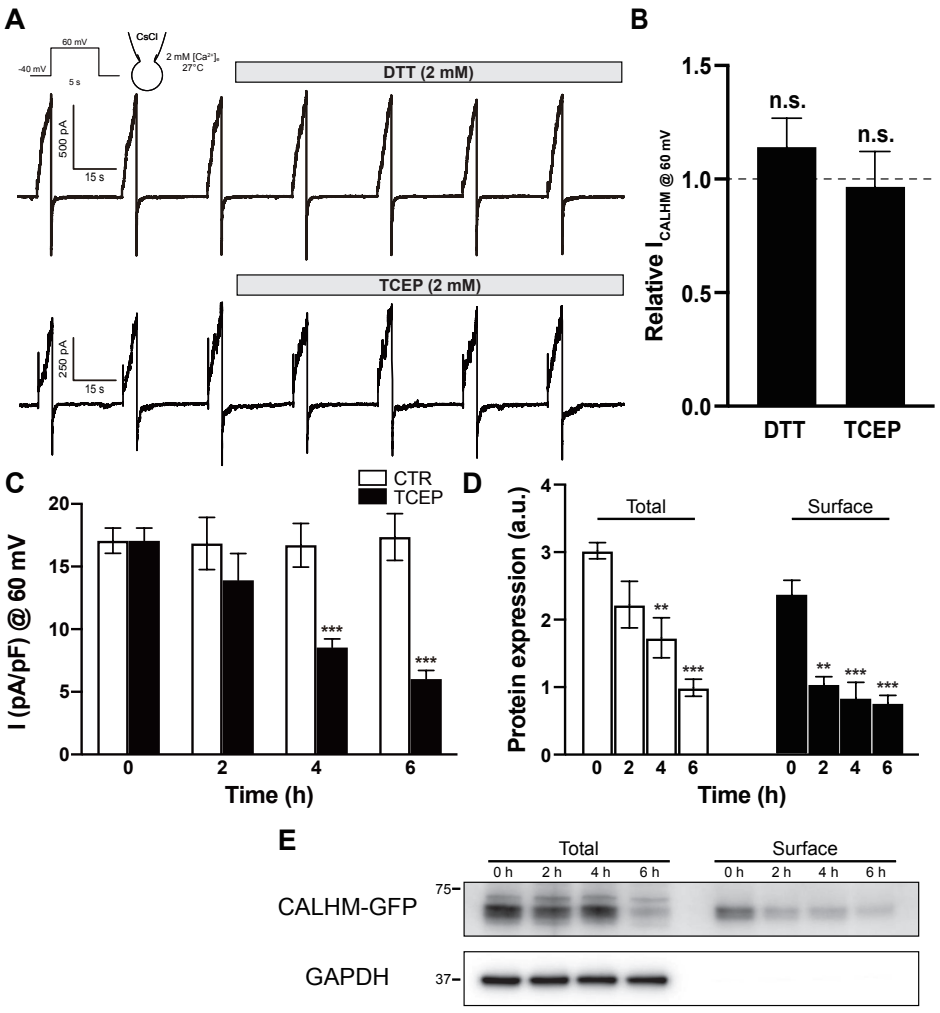

Fig. 6. Different effects of the acute and sustained treatment with reducing agent on I_{CALHM1} and protein expression. (A and B) Acute treatment with the reducing agents, DTT (2 mM, upper panel) and TCEP (2 mM, lower panel), did not change I_{CALHM1} under standard condition (2 mM $[Ca^{2+}]_e$ and 27°C). Representative trace (A) and summary of the current density (B) are shown (n = 8 and n = 13 for DTT and TCEP, respectively). n.s., not significant. (C) I_{CALHM1} gradually decreased following sustained treatment with cell-impermeable reducing agent, TCEP (n = 13 and n = 15 for control and TCEP, respectively). (D and E) CALHM1 membrane expression decreased markedly from 2 h after TCEP treatment (n = 5, closed bars). Total amount of CALHM1 expression levels also decreased when TCEP was treated, but the expression decreased gradually from 2 to 6 h (n = 5, open bars, one-way ANOVA; $**P < 0.01$, $***P < 0.001$).

surface biotinylation and immunoblotting analysis, CALHM1 expression decreased in the plasma membrane after 2 h of TCEP treatment (Figs. 6D and 6E). The expression had reduced even further 6 h after treatment. Interestingly, the total amount of CALHM1 protein also significantly decreased after 6 h of TCEP treatment.

DISCUSSION

The structures of various transmembrane proteins, including ion channels, are stabilized by intra- or intermolecular disulfide bonds. In the CALHM family, four cysteine residues were highly conserved across and within species (Fig. 1B). Recent cryo-EM studies have confirmed the intramolecular disulfide bridges investigated here (Choi et al., 2019; Demura et al., 2020; Ren et al., 2020; Yang et al., 2020). Although the cryo-EM structure of human CALHM1 has not been reported, we indirectly confirmed the existence of two disulfide bonds between four conserved cysteine residues using homology modeling of CALHM1 based on human CALHM2 structure. These disulfide bonds are located in the extracellular space and occur approximately 7 Å apart, when measured using the homology models and killifish CALHM1 cryo-EM structure. Interestingly, eight non-conserved cysteine residues were also located in CALHM1 cryo-EM structure, but the distances between them were too large to form intermolecular or intramolecular disulfide bridges (Fig. 1D). This implies that only the four conserved cysteine residues could form two intramolecular disulfide bonds (Figs. 1C-1E).

The nascent channel proteins are targeted to the endoplasmic reticulum (ER) and are folded and multimerized within the ER prior to membrane expression (Deutsch, 2003; Isacoff et al., 2013). In the ER, oxidative protein folding, a process of disulfide bond formation, and a conformational folding reaction are generated (Narayan, 2012). It is very important that only properly folded and assembled channels are trafficked to the plasma membrane as dysfunctional channels can have serious effects. Starting with ER quality control, maturation in Golgi shuttled channel complexes is also important to proceed in forward traffic to reach the cell membrane.

Our study showed the critical roles of the intramolecular disulfide bonds (C42-C127 and C44-C161) in the biogenesis and membrane trafficking of CALHM1 ion channels. Specifically, we found that the cysteine bridge between C44 and C161 (C44-C161) is essential, while that between C42 and C127 (C42-C127) is dispensable for multimerization in the

ER (Fig. 4). Nevertheless, the patch clamp and confocal microscopy demonstrated the necessity of both disulfide bonds as all mutants of the four individual cysteine residues showed impaired trafficking to the membrane, with no electrophysiological function (Figs. 2 and 3). We cautiously interpret that each disulfide bridge is critical to pass the quality check during CALHM1 localization to the plasma membrane.

While WT CALHM1 forms a homo-multimer, the single C42 mutation (C42S) lacking the C42-C127 bridge did not assemble into WT CALHM1 when it was co-expressed with WT CALHM1 (Figs. 5A and 5B). In addition, although CALHM1 and CALHM3 form a heteromeric ion channel (CALHM1/3) with higher activity than CALHM1 alone (Ma et al., 2018), the triple co-expression of WT CALHM1, CALHM3 and C42S CALHM1 did not affect the electrophysiological function (Figs. 5C and 5D). These results suggest that C42S might be unable to assemble with CALHM1/3 hetero-multimeric proteins.

Finally, we investigated the sensitivity of CALHM1 to DTT and TCEP. Surprisingly, despite the critical role of extracellular disulfide bridges in biogenesis and trafficking, I_{CALHM1} was not affected by acute treatment with both reducing agents (Figs. 6A and 6B). The absence of an acute response to the reducing agents indicated that, once assembled and trafficked to the membrane, the octameric CALHM1 channels can maintain their gating mechanisms even though the reducing agents may have reduced the extracellular disulfide bonds. Although there was possibility that the concentration of TCEP was not enough to break the extracellular disulfide bridges, we could not increase TCEP more than 2 mM due to toxic effects of reducing agent for maintaining tight seal.

Because TCEP is impermeable to the plasma membrane, we investigated the effect of sustained treatment on ion channel activity and membrane expression of CALHM1. We observed a decrease in I_{CALHM1} and the membrane expression of CALHM1 from 2-6 h, while GAPDH expression was unaltered (Figs. 6C-6E). We cautiously interpret that the conversion of disulfide bonds to sulfhydryl residues induced endocytic removal and impaired recycling to the plasma membrane. Furthermore, the disappearance of CALHM proteins in the total preparation suggested degradation of CALHM1 with reduced cysteines that would have lost structural integrity (Figs. 6D and 6E). Considering the effects of sustained treatment of TCEP on membrane expression, we carefully interpreted that 2 mM of TCEP could break disulfide bridge of CALHM1 channel, while absence of acute effects.

The time gap between the nonsignificant acute effect on I_{CALHM1} and the delayed decrease in expression stood out. Here, we interpret that the disconnected disulfide bridges affected the gating function while shortening the functional lifetime of the CALHM1 channels. Based on the limited information obtained from the present results, we could not exclude the possibility that the quaternary structural change in the CALHM1 channel due to TCEP treatment might be a slow phenomenon that could not be detected within several minutes by the patch clamp technique.

A number of studies have reported that intermolecular or inter subunit disulfide bridges are important for the assembly of ion channels; shaker-type voltage-gated K^+ channels (Schulteis et al., 1995; 1996), voltage-gated Na^+ channels (Chen et al., 2012; Yereddi et al., 2013), voltage-gated Ca^{2+} channels (Calderon-Rivera et al., 2012), voltage-gated H^+ channels (Fujiwara et al., 2013), and acid-sensing ion channels (Zha et al., 2009). Among the two-pore domain (K2P) K^+ channel family, TWIK1 and TREK1 form a heterodimeric channel via a disulfide bridge in the extracellular cap region (Hwang et al., 2014). However, the role of disulfide bridges in the cap structure formed by the extracellular M1-P1 linkers of each K2P monomer remains controversial (Zuniga and Zuniga, 2016).

The critical role of intramolecular disulfide bridges in functional channel expression has been reported in other types of ion channels; inward rectifier K^+ channels (Kir2.1 and 2.3) (Bannister et al., 1999; Cho et al., 2000), transient receptor potential channels (TRPC4 and 5) (Duan et al., 2018; 2019), transient receptor potential ankyrin channel (TRPA1) (Wang et al., 2012), TIM23 complex of mitochondria (Ramesh et al., 2016), chloride intracellular ion channel (CLIC1) (Al Khamici et al., 2016), and CALHM1, identified in this study. In contrast to the role of CALHM1 in membrane trafficking, the extracellular cysteine residues of Kir2.1 and 2.3 are required for their electrophysiological function but not for expression in the plasma membrane. Furthermore, the disulfide bond on the extracellular side of the pore and the preceding small loop of TRPC5 seem to be critical for the function and pharmacological activation of the agonist, Englerin A. The functional modulation of TRPC5 that results from changing the state of disulfide bonds using reducing agents has been reported (Xu et al., 2008). In contrast to TRPC5, acute treatment with a reducing agent did not affect I_{CALHM1}. However, the previously observed inhibitory effect of sustained TCEP treatment on TRPC5 activity (Hong et al., 2015) is similar to the results of the our present study, that is, reduction in I_{CALHM1} and membrane expression (Fig. 6).

As discussed above, the roles of disulfide bridges in channel complexes are widely variable and include biogenesis, gating process, and pharmacological modulation. Our study confirmed the essential role of highly conserved intramolecular disulfide bridges in the proper assembly and trafficking of CALHM1. Although TCEP treatment did not acutely change the channel activity, prolonged exposure to the reducing environment could significantly lower CALHM1 expression, and this might have pathophysiological implications in the cells and tissues where the functions of CALHM1 are being revealed.

ACKNOWLEDGMENTS

This work was supported by grants from the National Research Foundation of Korea (NRF-2018R1A5A2025964), EDISON (EDucation-research Integration through Simulation On the Net) Program (NRF-2016M3C1A6936605) and the Korea Health Technology R&D Project, through the Korea Health Industry Development Institute (KHIDI), funded by the Ministry of Health & Welfare, Republic of Korea (grant No. HP20C0199). This work was also supported by a grant from the M.D., Ph.D./Medical Scientist Training Programs through KHIDI to Y.K.J. We thank Prof. Chansik Hong for technical advices and helpful discussions.

AUTHOR CONTRIBUTIONS

J.W.K. and Y.K.J. conceived and performed the experiments. J.K. gave technical support. S.J.K. (Sang Jeong Kim) provided expertise and feedback. S.J.K. (Sung Joon Kim) wrote the manuscript and supervised the study.

CONFLICT OF INTEREST

The authors have no potential conflicts of interest to disclose.

ORCID

Jae Won Kwon https://orcid.org/0000-0002-4635-319X
Young Keul Jeon https://orcid.org/0000-0001-5200-380X
Jinsung Kim https://orcid.org/0000-0001-5135-3699
Sang Jeong Kim https://orcid.org/0000-0001-8931-3713
Sung Joon Kim https://orcid.org/0000-0002-0289-121X

REFERENCES

Al Khamici, H., Hossain, K.R., Cornell, B.A., and Valenzuela, S.M. (2016). Investigating sterol and redox regulation of the ion channel activity of CLIC1 using tethered bilayer membranes. Membranes (Basel) *6*, 51.

Bannister, J.P., Young, B.A., Sivaprasadarao, A., and Wray, D. (1999). Conserved extracellular cysteine residues in the inwardly rectifying potassium channel Kir2.3 are required for function but not expression in the membrane. FEBS Lett. *458*, 393-399.

Berman, J.M. and Awayda, M.S. (2013). Redox artifacts in electrophysiological recordings. Am. J. Physiol. Cell Physiol. *304*, C604-C613.

Calderon-Rivera, A., Andrade, A., Hernandez-Hernandez, O., Gonzalez-Ramirez, R., Sandoval, A., Rivera, M., Gomora, J.C., and Felix, R. (2012). Identification of a disulfide bridge essential for structure and function of the voltage-gated Ca(2+) channel alpha(2)delta-1 auxiliary subunit. Cell Calcium *51*, 22-30.

Chen, C., Calhoun, J.D., Zhang, Y., Lopez-Santiago, L., Zhou, N., Davis, T.H., Salzer, J.L., and Isom, L.L. (2012). Identification of the cysteine residue responsible for disulfide linkage of Na+ channel alpha and beta2 subunits. J. Biol. Chem. *287*, 39061-39069.

Cho, H.C., Tsushima, R.G., Nguyen, T.T., Guy, H.R., and Backx, P.H. (2000). Two critical cysteine residues implicated in disulfide bond formation and proper folding of Kir2.1. Biochemistry *39*, 4649-4657.

Choi, W., Clemente, N., Sun, W., Du, J., and Lu, W. (2019). The structures and gating mechanism of human calcium homeostasis modulator 2. Nature *576*, 163-167.

Demura, K., Kusakizako, T., Shihoya, W., Hiraizumi, M., Nomura, K., Shimada, H., Yamashita, K., Nishizawa, T., Taruno, A., and Nureki, O. (2020). Cryo-EM structures of calcium homeostasis modulator channels in diverse oligomeric assemblies. Sci. Adv. *6*, eaba8105.

Deutsch, C. (2003). The birth of a channel. Neuron *40*, 265-276.

Dreses-Werringloer, U., Lambert, J.C., Vingtdeux, V., Zhao, H., Vais, H., Siebert, A., Jain, A., Koppel, J., Rovelet-Lecrux, A., Hannequin, D., et al. (2008). A polymorphism in CALHM1 influences Ca^{2+} homeostasis, Abeta levels, and Alzheimer's disease risk. Cell *133*, 1149-1161.

Drozdzyk, K., Sawicka, M., Bahamonde-Santos, M.I., Jonas, Z., Deneka, D., Albrecht, C., and Dutzler, R. (2020). Cryo-EM structures and functional properties of CALHM channels of the human placenta. Elife *9*, e55853.

Duan, J., Li, J., Chen, G.L., Ge, Y., Liu, J., Xie, K., Peng, X., Zhou, W., Zhong, J., Zhang, Y., et al. (2019). Cryo-EM structure of TRPC5 at 2.8-A resolution reveals unique and conserved structural elements essential for channel function. Sci. Adv. *5*, eaaw7935.

Duan, J., Li, J., Zeng, B., Chen, G.L., Peng, X., Zhang, Y., Wang, J., Clapham, D.E., Li, Z., and Zhang, J. (2018). Structure of the mouse TRPC4 ion channel. Nat. Commun. *9*, 3102.

Foskett, J.K. (2020). Structures of CALHM channels revealed. Nat. Struct. Mol. Biol. *27*, 227-228.

Fujiwara, Y., Takeshita, K., Nakagawa, A., and Okamura, Y. (2013). Structural characteristics of the redox-sensing coiled coil in the voltage-gated H+ channel. J. Biol. Chem. *288*, 17968-17975.

Gamper, N., Stockand, J.D., and Shapiro, M.S. (2005). The use of Chinese hamster ovary (CHO) cells in the study of ion channels. J. Pharmacol. Toxicol. Methods *51*, 177-185.

Gibson, D.G., Young, L., Chuang, R.Y., Venter, J.C., Hutchison, C.A., 3rd, and Smith, H.O. (2009). Enzymatic assembly of DNA molecules up to several hundred kilobases. Nat. Methods *6*, 343-345.

Hong, C., Kwak, M., Myeong, J., Ha, K., Wie, J., Jeon, J.H., and So, I. (2015). Extracellular disulfide bridges stabilize TRPC5 dimerization, trafficking, and activity. Pflugers Arch. *467*, 703-712.

Hwang, E.M., Kim, E., Yarishkin, O., Woo, D.H., Han, K.S., Park, N., Bae, Y., Woo, J., Kim, D., Park, M., et al. (2014). A disulphide-linked heterodimer of TWIK-1 and TREK-1 mediates passive conductance in astrocytes. Nat. Commun. *5*, 3227.

Isacoff, E.Y., Jan, L.Y., and Minor, D.L., Jr. (2013). Conduits of life's spark: a perspective on ion channel research since the birth of neuron. Neuron *80*, 658-674.

Jeon, Y.K., Choi, S.W., Kwon, J.W., Woo, J., Choi, S.W., Kim, S.J., and Kim, S.J. (2021). Thermosensitivity of the voltage-dependent activation of calcium homeostasis modulator 1 (calhm1) ion channel. Biochem. Biophys. Res. Commun. *534*, 590-596.

Kashio, M., Wei-Qi, G., Ohsaki, Y., Kido, M.A., and Taruno, A. (2019). CALHM1/CALHM3 channel is intrinsically sorted to the basolateral membrane of epithelial cells including taste cells. Sci. Rep. *9*, 2681.

Ma, Z., Siebert, A.P., Cheung, K.H., Lee, R.J., Johnson, B., Cohen, A.S., Vingtdeux, V., Marambaud, P., and Foskett, J.K. (2012). Calcium homeostasis modulator 1 (CALHM1) is the pore-forming subunit of an ion channel that mediates extracellular Ca^{2+} regulation of neuronal excitability. Proc. Natl. Acad. Sci. U. S. A. *109*, E1963-E1971.

Ma, Z., Taruno, A., Ohmoto, M., Jyotaki, M., Lim, J.C., Miyazaki, H., Niisato, N., Marunaka, Y., Lee, R.J., Hoff, H., et al. (2018). CALHM3 is essential for rapid ion channel-mediated purinergic neurotransmission of GPCR-mediated tastes. Neuron *98*, 547-561.e10.

Narayan, M. (2012). Disulfide bonds: protein folding and subcellular protein trafficking. FEBS J. *279*, 2272-2282.

Okui, M., Murakami, T., Sun, H., Ikeshita, C., Kanamura, N., and Taruno, A. (2021). Posttranslational regulation of CALHM1/3 channel: N-linked glycosylation and S-palmitoylation. FASEB J. *35*, e21527.

Ramesh, A., Peleh, V., Martinez-Caballero, S., Wollweber, F., Sommer, F., van der Laan, M., Schroda, M., Alexander, R.T., Campo, M.L., and Herrmann, J.M. (2016). A disulfide bond in the TIM23 complex is crucial for voltage gating and mitochondrial protein import. J. Cell Biol. *214*, 417-431.

Ren, Y., Wen, T., Xi, Z., Li, S., Lu, J., Zhang, X., Yang, X., and Shen, Y. (2020). Cryo-EM structure of the calcium homeostasis modulator 1 channel. Sci. Adv. *6*, eaba8161.

Roh, J.W., Hwang, G.E., Kim, W.K., and Nam, J.H. (2021). Ca^{2+} sensitivity of anoctamin 6/TMEM16F is regulated by the putative Ca^{2+}-binding reservoir at the N-terminal domain. Mol. Cells *44*, 88-100.

Schulteis, C.T., John, S.A., Huang, Y., Tang, C.Y., and Papazian, D.M. (1995). Conserved cysteine residues in the shaker K+ channel are not linked by a disulfide bond. Biochemistry *34*, 1725-1733.

Schulteis, C.T., Nagaya, N., and Papazian, D.M. (1996). Intersubunit interaction between amino- and carboxyl-terminal cysteine residues in tetrameric shaker K+ channels. Biochemistry *35*, 12133-12140.

Syrjanen, J.L., Michalski, K., Chou, T.H., Grant, T., Rao, S., Simorowski, N.,

Tucker, S.J., Grigorieff, N., and Furukawa, H. (2020). Structure and assembly of calcium homeostasis modulator proteins. Nat. Struct. Mol. Biol. *27*, 150-159.

Tanis, J.E., Ma, Z., and Foskett, J.K. (2017). The NH_2 terminus regulates voltage-dependent gating of CALHM ion channels. Am. J. Physiol. Cell Physiol. *313*, C173-C186.

Taruno, A., Vingtdeux, V., Ohmoto, M., Ma, Z., Dvoryanchikov, G., Li, A., Adrien, L., Zhao, H., Leung, S., Abernethy, M., et al. (2013). CALHM1 ion channel mediates purinergic neurotransmission of sweet, bitter and umami tastes. Nature *495*, 223-226.

Thompson, J.D., Higgins, D.G., and Gibson, T.J. (1994). CLUSTAL W: improving the sensitivity of progressive multiple sequence alignment through sequence weighting, position-specific gap penalties and weight matrix choice. Nucleic Acids Res. *22*, 4673-4680.

Vingtdeux, V., Chang, E.H., Frattini, S.A., Zhao, H., Chandakkar, P., Adrien, L., Strohl, J.J., Gibson, E.L., Ohmoto, M., Matsumoto, I., et al. (2016). CALHM1 deficiency impairs cerebral neuron activity and memory flexibility in mice. Sci. Rep. *6*, 24250.

Wang, L., Cvetkov, T.L., Chance, M.R., and Moiseenkova-Bell, V.Y. (2012). Identification of in vivo disulfide conformation of TRPA1 ion channel. J. Biol. Chem. *287*, 6169-6176.

Waterhouse, A., Bertoni, M., Bienert, S., Studer, G., Tauriello, G., Gumienny, R., Heer, F.T., de Beer, T.A.P., Rempfer, C., Bordoli, L., et al. (2018). SWISS-MODEL: homology modelling of protein structures and complexes. Nucleic Acids Res. *46*(W1), W296-W303.

Xu, S.Z., Sukumar, P., Zeng, F., Li, J., Jairaman, A., English, A., Naylor, J., Ciurtin, C., Majeed, Y., Milligan, C.J., et al. (2008). TRPC channel activation by extracellular thioredoxin. Nature *451*, 69-72.

Yang, W., Wang, Y., Guo, J., He, L., Zhou, Y., Zheng, H., Liu, Z., Zhu, P., and Zhang, X.C. (2020). Cryo-electron microscopy structure of CLHM1 ion channel from Caenorhabditis elegans. Protein Sci. *29*, 1803-1815.

Yereddi, N.R., Cusdin, F.S., Namadurai, S., Packman, L.C., Monie, T.P., Slavny, P., Clare, J.J., Powell, A.J., and Jackson, A.P. (2013). The immunoglobulin domain of the sodium channel beta3 subunit contains a surface-localized disulfide bond that is required for homophilic binding. FASEB J. *27*, 568-580.

Zha, X.M., Wang, R., Collier, D.M., Snyder, P.M., Wemmie, J.A., and Welsh, M.J. (2009). Oxidant regulated inter-subunit disulfide bond formation between ASIC1a subunits. Proc. Natl. Acad. Sci. U. S. A. *106*, 3573-3578.

Zuniga, L. and Zuniga, R. (2016). Understanding the cap structure in K2P channels. Front. Physiol. *7*, 228.